

# Stability Analysis of Fractional Order Memristor Synapse-coupled Hopfield Neural Network with Ring Structure

Leila Eftekhari<sup>a</sup>, Mohammad M. Amirian<sup>b,\*</sup>

<sup>a</sup>*Department of Mathematics, Tarbiat Modares University, Tehran, IR 14117-13116*

<sup>b</sup>*Department of Mathematics and Statistics, Dalhousie University, Halifax, NS, CA B3H4R2*

---

## Abstract

A memristor is a nonlinear two-terminal electrical element that incorporates memory features and nanoscale properties, enabling us to design very high-density artificial neural networks. To enhance the memory property, we should use mathematical frameworks like fractional calculus, which is capable of doing so. Here, we first present a fractional-order memristor synapse-coupling Hopfield neural network on two neurons and then extend the model to a neural network with a ring structure that consists of  $n$  sub-network neurons, increasing the synchronization in the network. Necessary and sufficient conditions for the stability of equilibrium points are investigated, highlighting the dependency of the stability on the fractional-order value and the number of neurons. Numerical simulations and bifurcation analysis, along with Lyapunov exponents, are given in the two-neuron case that substantiates the theoretical findings, suggesting possible routes towards chaos when the fractional order of the system increases. In the  $n$ -neuron case also, it is revealed that the stability depends on the structure and number of sub-networks.

**Keywords:** Fractional Calculus, Bifurcation, Stability, Memristor, Hopfield Neural Network

---

## 1. Introduction

The brain as the central organ of the nervous system regulates most of the activities in our body. Brain dynamics is generally studied based on mathematical equations and frameworks, more specifically artificial neural networks models [1–4]. Artificial neural networks can mimic the complex behaviour of non-linear systems like fractional calculus. Fractional calculus is a generalised version of integer calculus and a specific case of convolution integral [5]. Lately, there has been some promising progress in solving fractional differential equations using artificial neural networks [6–9]. Zúñiga-Aguilar et al have recently suggested a new method using neural networks, optimized by the Levenberg–Marquardt algorithm, to solve fractal-fractional differential equations with a non-singular and non-local kernel [10]. Aguilar et al used a fractionalized version of

---

\*

*Email address:* M.Amiriammatlob@dal.ca (Mohammad M. Amirian)

neural networks to study system identification, and they have found that their model has a higher precision with a fewer number of parameters compared to integer models [11]. Among artificial neural networks models, Hopfield neural network (HNN) draws considerable attention due to its simple paradigm in designing the systems that provide us with a better understanding of human memory [12, 13]. HNN has a wide range of applications in artificial intelligence, such as machine learning, associative memory, pattern recognition including self-excited hyperchaotic and chaotic oscillations [14], period-adding bifurcations [15], and coexisting asymmetric multi-stable [16] patterns, optimized calculation, VLSI and parallel realization of optical devices [17, 18].

Memristors can be used to forecast electromagnetic induction in biological systems, neuronal simulations, and complex systems with learning and forgetting mechanisms [19]. Using memristors instead of resistors in the Hopfield neural network models, for instance, one can build a new system where the parameters vary according to their state variables, which is said to be a memristor-based neural network. This component can also be implemented by well-known models such as Hodgkin–Huxley [20, 21], Hindmarsh–Rose [22], Morris–Lecar [23], Rulkov [24], and Wilson neuronal model [25, 26] to study the specific phenomena of interest. To enrich the non-linear behaviour of biological neurons, for example, H. Bao et al used a Hindmarsh–Rose neuronal model, thereby representing the complex dynamical features of the electrical activities better [27]. It is worth noting that the action potential in the models could be affected by the choice activation functions, such as hyperbolic tangent function, exponential function, non-monotonous activation, piecewise-linear, etc [28]. Here we are using hyperbolic tangent function.

The memory features and nanoscale properties of the memristor enable us to design very high-density systems. This component can be used as synaptic weights in artificial neural networks due to their learning ability [29]. Depending on the question of interest in artificial neural network models, different types of network topology could be used to uncover a desirable output [30, 31]. One commonly-used network topology is ring topology. The ring network creates an ongoing pathway for signals through each node, connected to two other nodes, and it has been implemented in many fields such as circuits, mobile ad hoc networks and optical networks [32–35].

Unlike ordinary calculus, definitions in fractional calculus are not unique. In fractional calculus, we have various operators under different weight functions, giving us a wide range of opportunities to study complex systems incorporating memory properties on the one hand [5, 36–40] and rising computational barriers problems on the other hand [41]. Some basic theorems and algebra lemmas such as chain rule and stability criteria holding for integer calculus is no longer valid when it comes to fractional calculus [5, 42]. Therefore, careful attention is required to control the dynamics of fractional network models. This paper aims to build up a solid mathematical framework for the stability criteria of  $n$ -dimensional fractional-order network models. To do so, we first introduce our fractional-order memristor synapse-coupled Hop-field neural network (FMHNN) on two neurons using fractional derivative in sense of Caputo (Eq. 4). We chose this fractional operator since it only requires initial conditions given in terms of integer-order

derivatives [42], consisting with the property of our model. Applying the ring network concept on equations, we then expand our model to a more complex system, where each membrane is coupled by  $n$  sub-networks. After building the required fundamental theoretical bases for stability analysis, we examine the criteria numerically for both systems and perform bifurcation analysis, investigating the impact of the initial condition on FMHNN model.

## 2. Materials and Methods

### 2.1. Models

**FMHNN Model.** Using the definition (2.1), we extend the concept of the integer-order memristor synapse-coupled Hopfield neural network (MHNN), represented in 2019 [43], to FMHNN in the following form

$$\begin{cases} {}^C_0D_t^\alpha x_1 = -x_1 + b_1 \tanh(x_1) + b_2 \tanh(x_2) + k\varphi(x_1 - x_2), \\ {}^C_0D_t^\alpha x_2 = -x_2 + b_3 \tanh(x_1) + b_4 \tanh(x_2) - k\varphi(x_1 - x_2), \\ {}^C_0D_t^\alpha \varphi = x_1 - x_2. \end{cases} \quad (1)$$

where  $0 < \alpha \leq 1$  is the fractional order, and  $b_i$  are constant parameters. Note that the FMHNN model reduces to MHNN model when  $\alpha = 1$ .

In this model, when there is a potential difference between the neurons, an induction current will appear, and a two-way induction current  $I_M$  flows through an active flux controlled memristor synapse as shown below

$$\begin{cases} I_M = W(\varphi)V_M = k\varphi V_M, \\ \varphi = f(V_M) = V_M. \end{cases} \quad (2)$$

where  $\varphi$  and  $V_M$  account for the state variable of the memristor, and the potential difference of the two neurons, respectively;  $W = k\varphi$  also explains a memductance function with memristor coupling weight  $k$ .  $x_1$  and  $x_2$  are the state variables describing the potentials between the inside and outside of the two neurons,  $\tanh(x_1)$  and  $\tanh(x_2)$  are the activation function of the two neurons, and  $V_M = x_1 - x_2$  is the potential difference of the two neurons. The coefficients represent the amplitude of a connection between two neurons. The FMHNN schematic connection pattern of two neurons is shown in Fig (1).

**FMHNN Model with Ring Structure.** We apply a ring-network structure on FMHNN model (1), and by doing so we expand our previous model from two neurons to  $n$  units of neurons. The ring network consists of  $n$  sub-networks coupling strength

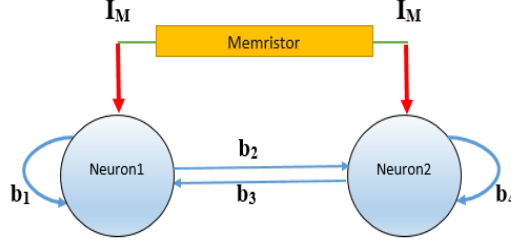


Figure 1: The FMHNN connection pattern with two neurons.

among all membrane potentials  $x_{1i}$  in the following form

$$\begin{cases} {}^c_0D_t^\alpha x_{1i} &= -x_{1i} + b_1 \tanh(x_{1i}) + b_2 \tanh(x_{2i}) + k\varphi_i(x_{1i} - x_{2i}) + \frac{d}{2p} \sum_{j=i-p}^{i+p} (x_{1j} - x_{1i}), \\ {}^c_0D_t^\alpha x_{2i} &= -x_{2i} + b_3 \tanh(x_{1i}) + b_4 \tanh(x_{2i}) - k\varphi_i(x_{1i} - x_{2i}), \\ {}^c_0D_t^\alpha \varphi_i &= x_{1i} - x_{2i}. \end{cases} \quad (3)$$

where  $i = 1, 2, \dots, n$ , and  $[x_{1i}, x_{2i}, \varphi_i]$  represent the state variables of  $i^{th}$  sub-network. Further, the memristor synapses are coupled symmetrically to their  $2P$  nearest neighbourhood by neural sub-networks, interacting with  $P$  neighbourhood from of left and right side. Also,  $d$  stands for the coupling strength among the  $n$  sub-networks.

**Definition 2.1.** [41] For a continuous function  $f$ , with  $f' \in L^1(R^+)$ , the Caputo fractional-order derivative of order  $\alpha \in (0, 1)$  is defined by

$${}^c_{t_0}D_t^\alpha f(t) = \frac{1}{\Gamma(1-\alpha)} \int_{t_0}^t (t-s)^{-\alpha} f'(s) ds. \quad (4)$$

## 2.2. Model Analysis

Here, we study the existence and uniqueness of solutions and determine the stability criteria for both models (1 & 3). To do so, some fundamental definitions are required; each subsection therefore starts with those information.

### 2.2.1. Existence and Uniqueness of Solutions

**Definition 2.2.** The **circulant matrix** is a square matrix in which each row has the previous row components shifted cyclically one place towards the right side.

$$B = \text{circ}(b_0, b_1, \dots, b_{n-1}) = \begin{bmatrix} b_0 & b_1 & b_2 & b_3 & \cdots & b_{n-2} & b_{n-1} \\ b_{n-1} & b_0 & b_1 & b_2 & \cdots & b_{n-3} & b_{n-2} \\ b_{n-2} & b_{n-1} & b_0 & b_1 & \cdots & b_{n-4} & b_{n-3} \\ \cdots & \cdots & \cdots & \cdots & \cdots & \cdots & \cdots \\ b_2 & b_3 & b_4 & b_5 & \cdots & b_0 & b_1 \\ b_1 & b_2 & b_3 & b_4 & \cdots & b_{n-1} & b_0 \end{bmatrix}_{n \times n}.$$

Also, the **block circulant matrix** is the generalized version of the above matrix where each component consist of the circulant matrix

$$B = \text{bcirc}(B_0, B_1, \dots, B_{n-1}) = \begin{bmatrix} B_0 & B_1 & B_2 & B_3 & \cdots & B_{n-2} & B_{n-1} \\ B_{n-1} & B_0 & B_1 & B_2 & \cdots & B_{n-3} & B_{n-2} \\ B_{n-2} & B_{n-1} & B_0 & B_1 & \cdots & B_{n-4} & B_{n-3} \\ \cdots & \cdots & \cdots & \cdots & \cdots & \cdots & \cdots \\ B_2 & B_3 & B_4 & B_5 & \cdots & B_0 & b_1 \\ B_1 & B_2 & B_3 & B_4 & \cdots & B_{n-1} & B_0 \end{bmatrix}_{n \times n}.$$

which  $B_i$  (for  $i = 0, \dots, n-1$ ) is a block matrices [44, 45].

**Theorem 2.1.** Assume that  $\Omega = \{(x_1, x_2, \varphi) \in R^3 : \max\{|\varphi|\} \leq \lambda\}$  and  $S = \Omega \times [t_0, T]$  where  $T < \infty$ . For any initial conditions  $(x_1(t_0), x_2(t_0), \varphi(t_0)) \in \Omega$ , all the solutions  $(x_1(t), x_2(t), \varphi(t)) \in S$  of system (1) are unique for all  $t \geq 0$ .

*Proof.* Let  $\mathbb{F}(x) = (\mathbb{F}_1(x), \mathbb{F}_2(x), \mathbb{F}_3(x))^T$  be a mapping function with  $\|\cdot\|$  norm so that

$$\begin{aligned} \mathbb{F}_1(x) &= -x_1 + b_1 \tanh(x_1) + b_2 \tanh(x_2) + k\varphi(x_1 - x_2), \\ \mathbb{F}_2(x) &= -x_2 + b_3 \tanh(x_1) + b_4 \tanh(x_2) - k\varphi(x_1 - x_2), \\ \mathbb{F}_3(x) &= x_1 - x_2 \end{aligned}$$

where  $x = (x_1, x_2, \varphi)$ . Therefore, we can re-write our mapping function in a multi-variable form,  $\mathbb{F}(x) = Ax + B \tanh(x) + \varphi Kx$ , such that

$$A = \begin{bmatrix} -1 & 0 & 0 \\ 0 & -1 & 0 \\ 1 & -1 & 0 \end{bmatrix}, \quad B = \begin{bmatrix} b_1 & b_2 & 0 \\ b_3 & b_4 & 0 \\ 0 & 0 & 0 \end{bmatrix}, \quad K = \begin{bmatrix} k & -k & 0 \\ -k & k & 0 \\ 0 & 0 & 0 \end{bmatrix}, \quad x = \begin{bmatrix} x_1 \\ x_2 \\ \varphi \end{bmatrix}$$

We now prove that the system (1) satisfies the locally Lipschitz condition [36], i.e.

$$\forall \mathbf{x}, \bar{\mathbf{x}} \in S, \exists L \geq 0 \quad \text{s.t.} \quad \|\mathbb{F}(\mathbf{x}) - \mathbb{F}(\bar{\mathbf{x}})\| \leq L\|\mathbf{x} - \bar{\mathbf{x}}\|$$

where  $\mathbf{x} = (x_1, x_2, \varphi)^T$  and  $\bar{\mathbf{x}} = (\bar{x}_1, \bar{x}_2, \bar{\varphi})^T$ .

$$\begin{aligned} \|\mathbb{F}(\mathbf{x}) - \mathbb{F}(\bar{\mathbf{x}})\| &= \|A(\mathbf{x} - \bar{\mathbf{x}}) + B(\tanh(\mathbf{x}) - \tanh(\bar{\mathbf{x}})) + K(\varphi\mathbf{x} - \bar{\varphi}\bar{\mathbf{x}})\| \\ &\leq \|A\| \|\mathbf{x} - \bar{\mathbf{x}}\| + \|B\| \|\tanh(\mathbf{x}) - \tanh(\bar{\mathbf{x}})\| + \|K\varphi\| \|\mathbf{x} - \bar{\mathbf{x}}\| \\ &\leq (\|A\| + \|B\| + \|K\| \|\varphi\|) \|\mathbf{x} - \bar{\mathbf{x}}\| \\ &\leq (\|A\| + \|B\| + \lambda\|K\|) \|\mathbf{x} - \bar{\mathbf{x}}\| \\ &= L\|\mathbf{x} - \bar{\mathbf{x}}\| \end{aligned}$$

where  $L = (\|A\| + \|B\| + \lambda\|K\|) > 0$ . This means that with an initial condition  $\mathbf{x}(t_0) = (x_1(t_0), x_2(t_0), \varphi(t_0))^T$ , FMHNN model (1) has an unique solution  $\mathbf{x}(t) \in S$ .  $\square$

**Theorem 2.2.** Assume that  $\Omega = \{(\mathbf{x}_1, \mathbf{x}_2, \phi) \in \mathbb{R}^{n \times 3}, \text{ s.t. } \mathbf{x}_1 = [x_{1i}]_{n \times 1}, \mathbf{x}_2 = [x_{2i}]_{n \times 1}, \phi = [\varphi_i]_{n \times 1}, \Lambda = [\lambda_i]_{n \times 1}, \max\{|\phi|\} \leq \Lambda\}_{i=1,2,\dots,n}$  and also  $S = \Omega \times [T_0, T]$  where  $T = [T_i]_{n \times 1}$ ,  $T_0 = [t_{0i}]_{n \times 1}$  for  $i = 1, 2, \dots, n$  and  $T < \infty$ . For any initial conditions  $(\mathbf{x}_1(T_0), \mathbf{x}_2(T_0), \phi(T_0)) \in \Omega$ , all the solutions  $(\mathbf{x}_1(T), \mathbf{x}_2(T), \phi(T)) \in S$  of system (3) are unique for all  $T \geq 0$ .

*Proof.* Let  $\mathbb{F}(\mathbf{X}) = (\mathbb{F}_1(\mathbf{X}), \mathbb{F}_2(\mathbf{X}), \mathbb{F}_3(\mathbf{X}))^T$  be a multi-variable mapping function with  $\|\cdot\|$  norm so that

$$\begin{aligned} \mathbb{F}_1(\mathbf{X}) &= -\mathbf{x}_1 + b_1 \tanh(\mathbf{x}_1) + b_2 \tanh(\mathbf{x}_2) + k\varphi(\mathbf{x}_1 - \mathbf{x}_2) + \frac{d}{2p} \sum_{j=i-p}^{i+p} (\mathbf{x}_{1j} - \mathbf{x}_{1i}), \\ \mathbb{F}_2(\mathbf{X}) &= -\mathbf{x}_2 + b_3 \tanh(\mathbf{x}_1) + b_4 \tanh(\mathbf{x}_2) - k\varphi(\mathbf{x}_1 - \mathbf{x}_2), \\ \mathbb{F}_3(\mathbf{X}) &= \mathbf{x}_1 - \mathbf{x}_2. \end{aligned} \tag{5}$$

Therefore, we can re-write our mapping function in the following form

$$\mathbb{F}(\mathbf{X}) = A\mathbf{X} + B_1 \tanh(\mathbf{X}) + B_2 \tanh(\mathbf{X}) + \varphi K\mathbf{X},$$

where  $A = \text{bcirc}(A_0, A_1, \dots, A_1) \in \mathbb{R}^{n \times n}$ ,  $B_1 = [\beta_1]_{1 \times n}$ ,  $B_2 = [\beta_2]_{1 \times n}$ ,  $\beta_1 = [b_1, b_3, 0]$ ,  $\beta_2 = [b_2, b_4, 0]$ , and  $K = \text{bcirc}(\kappa, 0, \dots, 0)_{1 \times n}$  so that  $A_0, A_1 \in \mathbb{R}^{3 \times 3}$  and

$$A_0 = \begin{bmatrix} -1 - \frac{d}{p} & 0 & 0 \\ 0 & -1 & 0 \\ 1 & -1 & 0 \end{bmatrix}, \quad A_1 = \begin{bmatrix} \frac{d}{2p} & 0 & 0 \\ 0 & 0 & 0 \\ 0 & 0 & 0 \end{bmatrix}, \quad \kappa = \begin{bmatrix} -k & k & 0 \\ k & -k & 0 \\ 0 & 0 & 0 \end{bmatrix}$$

We now prove that the system (3) satisfies the locally Lipschitz condition [36], i.e.

$$\forall \mathbf{X}, \bar{\mathbf{X}} \in S, \exists L \geq 0 \quad \text{s.t.} \quad \|\mathbb{F}(\mathbf{X}) - \mathbb{F}(\bar{\mathbf{X}})\| \leq L\|\mathbf{X} - \bar{\mathbf{X}}\|,$$

$$\begin{aligned}
\|\mathbb{F}(X) - \mathbb{F}(\bar{X})\| &= \|A(X - \bar{X}) + (B_1 + B_2)(\tanh(X) - \tanh(\bar{X})) + K(\varphi X - \bar{\varphi}\bar{X})\| \\
&\leq \|A\| \|X - \bar{X}\| + \|B_1 + B_2\| \|\tanh(X) - \tanh(\bar{X})\| + \|\Lambda\| \|K\| \|X - \bar{X}\| \\
&\leq (\|A\| + \|B_1\| + \|B_2\| + \|\Lambda\| \|K\|) \|X - \bar{X}\| \\
&= L\|X - \bar{X}\|,
\end{aligned}$$

where  $L = (\|A\| + \|B_1\| + \|B_2\| + \|\Lambda\| \|K\|)$ . This means that with an initial condition  $X(t_0) = (x_1(t_0), x_2(t_0), \phi(t_0))^T$ , FMHNN model with ring structure (3) has a unique solution  $X(t) \in S$ .  $\square$

### 2.2.2. Stability of Solutions

Here, we build up the theoretical framework for the stability analysis of our models.

**Definition 2.3.** [5] For  $0 < \alpha < 1$ , the Laplace transform of Caputo fractional derivative,  ${}^C_{t_0}D_t^\alpha f(t)$ , derives from the following equation

$$\int_0^\infty e^{-st} {}^C_{t_0}D_t^\alpha f(t) dt = s^\alpha F(s) - s^{\alpha-1} f(t_0)$$

**Definition 2.4.** [5] For matrix  $A \in R^{n \times n}$ , the matrix Mittag-Leffler function is defined by

$$E_{\alpha, \beta}[A] = \sum_{k=0}^{\infty} \frac{A^k}{\Gamma(\alpha k + \beta)}$$

**Lemma 2.1.** [46] The linear autonomous system  ${}^C_{t_0}D_t^\alpha x = Ax$  is asymptotically stable if and only if

$$|\arg(\lambda)| > \frac{\alpha\pi}{2} \text{ when } \lambda \in \sigma(A) \quad (6)$$

where  $\sigma(A)$  denotes the spectrum of the matrix  $A \in R^{n \times n}$ .

**Lemma 2.2.** [47] The roots of the second order polynomial  $p(\lambda) = \lambda^2 + a\lambda + c$  satisfies inequality (6) if and only if  $c > 0$  and  $b/\sqrt{c} < 2 \cos(\alpha\pi/2)$ .

**Lemma 2.3.** [42] If  $A \in R^{n \times n}$ ,  $\beta$  is an arbitrary real number, and  $\frac{\alpha\pi}{2} < \mu < \min\{\pi, \alpha\pi\}$ , then a real positive constant,  $r > 0$ , exists so that

$$\|E_{\alpha, \beta}[A]\| \leq \frac{r}{1 + \|A\|}, \quad \mu \leq |\arg(\lambda_i[A])| \leq \pi, \text{ for } i = 1, 2, \dots, n \quad (7)$$

where  $\lambda_i(A)$  denotes the eigenvalues of matrix  $A$ .

**Lemma 2.4.** [48] Assume that  $u(t)$  and  $f(t)$  are real-valued piecewise-continuous functions defined on the real interval  $[a, b]$ ,  $K(t)$  is also real-valued and  $K(t) \in L(a, b)$  and

$u(t)$ ,  $K(t)$  are non-negative on this interval.

$$\forall t \in [a, b], \quad u(t) \leq f(t) + \int_a^t K(\tau)u(\tau)d\tau$$

and

$$u(t) \leq f(t) + \int_a^t f(\tau)K(\tau)u(\tau) \exp \left\{ \int_\tau^t K(s)ds \right\} d\tau.$$

**Theorem 2.3.** Assume that we are given the following fractional order system with non-zero initial condition,  $\mathbf{x}(t_0) = \mathbf{x}_0$  :

$${}^C_{t_0}D_t^\alpha \mathbf{x}(t) = A\mathbf{x}(t) + \mathbb{H}[\mathbf{x}(t)] \quad (8)$$

where  $0 < \alpha \leq 1$ ,  $A \in R^{n \times n}$  is a constant matrix,  $\mathbf{x} = (x_1, x_2, \dots, x_n)^T \in R^{n \times 1}$  is the state vector of our fractional-order system,  ${}^C_{t_0}D_t^\alpha \mathbf{x}(t)$ , which consists of the linear  $A\mathbf{x}(t)$  and nonlinear  $\mathbb{H}[\mathbf{x}(t)]$  parts. System (8) is locally asymptotically stable at its equilibrium point,  $\mathbf{x}^*$ , when

$$|\arg(\lambda_i)| > \alpha \frac{\pi}{2}, \quad \text{and} \quad \lim_{\mathbf{x} \rightarrow \mathbf{x}^*} \frac{\|\mathbb{H}[\mathbf{x}(t)]\|}{\|\mathbf{x} - \mathbf{x}^*\|} = 0$$

where  $\lambda_i$  ( $i = 1, 2, \dots, n$ ) is the eigenvalues of matrix  $A$ .

*Proof.* The equation (8) can be written in the following form after taking Laplace transform from it.

$$s^\alpha \mathbf{X}(s) - s^{\alpha-1} \mathbf{x}_0 = A\mathbf{X}(s) + L\{\mathbb{H}[\mathbf{x}(t)]\}$$

Thus

$$\mathbf{X}(s) = (s^\alpha I - A)^{-1} [s^{\alpha-1} \mathbf{x}_0 + L\{\mathbb{H}[(\mathbf{x}(t))]\},$$

where  $I$  is an  $n \times n$  identity matrix. After taking Laplace inverse transform from the above equation (Table C1 of [5]), we would have

$$\mathbf{x}(t) = E_{\alpha,1}(At^\alpha)\mathbf{x}_0 + \int_0^t (t-\tau)^{\alpha-1} E_{\alpha,\alpha}(A(t-\tau)^\alpha) \mathbb{H}[\mathbf{x}(\tau)] d\tau,$$

Let  $\mathbf{x}^*$  be the solution of system (8) and  $\lim_{\mathbf{x} \rightarrow \mathbf{x}^*} \frac{\|\mathbb{H}[\mathbf{x}(t)]\|}{\|\mathbf{x} - \mathbf{x}^*\|} = 0$ . Therefore

$$\forall \varepsilon > 0 \exists \delta_0 > 0 \text{ s.t. } \|\mathbf{x}(t) - \mathbf{x}^*\| < \delta_0 \Rightarrow \|\mathbb{H}[\mathbf{x}(t)]\| < \varepsilon \|\mathbf{x} - \mathbf{x}^*\|$$

Now let  $\delta$  be chosen arbitrarily subject to  $0 < \delta < \delta_0$  and consider solutions for which



$\|x_0\| < \delta$ . From lemma (2.3)

$$\exists r_0, r \in R^+ \text{ s.t. } \|x(t) - x^*\| \leq \frac{r_0 \|x_0\|}{1 + \|A\| t^\alpha} + \int_0^t \frac{\varepsilon r_0 r (t - \tau)^{\alpha-1}}{(1 + \|A\| (t - \tau)^\alpha)} \|x(\tau) - x^*\| d\tau,$$

Using Grönwall's inequality Lemma (2.4) and letting  $\epsilon = \varepsilon r_0 r \delta_0$ , we would have

$$\begin{aligned} \|x(t) - x^*\| &\leq \frac{r_0 \|x_0\|}{1 + \|A\| t^\alpha} + \int_0^t \frac{\epsilon \|x(t)\|}{1 + \|A\| \tau^\alpha} \frac{(t - \tau)^{\alpha-1}}{(1 + \|A\| (t - \tau)^\alpha)} \times \exp \left\{ \int_\tau^t \frac{(t - s)^{\alpha-1}}{(1 + \|A\| (t - s)^\alpha)} ds \right\} d\tau \\ &\leq \frac{r_0 \|x_0\|}{1 + \|A\| t^\alpha} + \int_0^t \frac{\epsilon \|x_0\| (t - \tau)^{\alpha-1}}{(1 + \|A\| \tau^\alpha)(1 + \|A\| (t - \tau)^\alpha)^{1-1/\alpha\|A\|}} d\tau, \end{aligned}$$

The integral equals to the sum of the two parts

$$\begin{aligned} \int_0^t \frac{\epsilon \|x_0\| (t - \tau)^{\alpha-1}}{(1 + \|A\| \tau^\alpha)(1 + \|A\| (t - \tau)^\alpha)^{1-1/\alpha\|A\|}} d\tau &= \int_0^{t/2} \frac{\epsilon \|x_0\| (t - \tau)^{\alpha-1}}{(1 + \|A\| \tau^\alpha)(1 + \|A\| (t - \tau)^\alpha)^{1-1/\alpha\|A\|}} d\tau \\ &\quad + \int_{t/2}^t \frac{\epsilon \|x_0\| (t - \tau)^{\alpha-1}}{(1 + \|A\| \tau^\alpha)(1 + \|A\| (t - \tau)^\alpha)^{1-1/\alpha\|A\|}} d\tau \end{aligned}$$

Since  $\alpha < 1$  and  $(t - \tau) \geq \tau$  when  $\tau \in [0, t/2]$ , we would have

$$\int_0^{t/2} \frac{\epsilon \|x_0\| (t - \tau)^{\alpha-1}}{(1 + \|A\| (t - \tau)^\alpha)(1 + \|A\| \tau^\alpha)^{1-1/\alpha\|A\|}} d\tau \leq \int_0^{t/2} \frac{\epsilon \|x_0\| (\tau)^{\alpha-1}}{(1 + \|A\| \tau^\alpha)(1 + \|A\| \tau^\alpha)^{1-1/\alpha\|A\|}} d\tau$$

Similarly

$$\begin{aligned} \int_{t/2}^t \frac{\epsilon \|x_0\| (t - \tau)^{\alpha-1}}{(1 + \|A\| \tau^\alpha)(1 + \|A\| (t - \tau)^\alpha)^{1-1/\alpha\|A\|}} d\tau &\leq \int_{t/2}^t \frac{\epsilon \|x_0\| (t - \tau)^{\alpha-1}}{(1 + \|A\| (t - \tau)^\alpha)(1 + \|A\| (t - \tau)^\alpha)^{1-1/\alpha\|A\|}} d\tau \\ &= \int_{t/2}^t \frac{\epsilon \|x_0\| s^{\alpha-1}}{(1 + \|A\| s^\alpha)(1 + \|A\| s^\alpha)^{1-1/\alpha\|A\|}} ds \end{aligned}$$

By substituting  $s$  for  $(t - \tau)$  and by considering  $|\arg(\lambda_i)| > \alpha \frac{\pi}{2}$ , we would have  $\alpha \|A\| > 1$ ,

resulting in the following inequality

$$\begin{aligned} \|x(t) - x^*\| &\leq \frac{r_0 \|x_0\|}{1 + \|A\| t^\alpha} + 2 \int_0^{t/2} \frac{\epsilon \|x_0\|}{(1 + \|A\| \tau^\alpha)^{(2-1/\alpha)\|A\|}} d\tau, \\ &= \frac{r_0 \|x_0\|}{1 + \|A\| t^\alpha} + \frac{2\epsilon \|x_0\|}{\alpha \|A\| - 1} + \frac{2\epsilon \|x_0\|}{(1 - \alpha \|A\|)(1 + \|A\| (\frac{t}{2})^\alpha)^{1-1/\alpha\|A\|}} \end{aligned}$$

Since  $\delta$  and  $\delta_0$  are arbitrarily small, we would have

$$\lim_{t \rightarrow \infty} \left( \frac{r_0 \|x_0\|}{1 + \|A\| t^\alpha} + \frac{2\epsilon \|x_0\|}{\alpha \|A\| - 1} + \frac{2\epsilon \|x_0\|}{(1 - \alpha \|A\|)(1 + \|A\| (\frac{t}{2})^\alpha)^{1-1/\alpha\|A\|}} \right) = 0$$

Therefore, the solution of system (8) is asymptotically stable.  $\square$

**Remark 2.1.** Let  $B = bcirc(A, C, \dots, C) \in \mathbb{C}^{N \times N}$  then

$$\lambda(B) = \left\{ \lambda(A + (N-1)C), \underbrace{\lambda(A-C), \dots, \lambda(A-C)}_{N-1} \right\}$$

### 2.2.3. Stability of FMHNN Model

**Theorem 2.4.** The system (1) is asymptotically stable at its equilibrium point,  $E^* = [0, 0, \delta]$ , if and only if one of the following conditions hold

$$i. \eta > 0 \text{ and } \frac{\tau}{\sqrt{\eta}} < 2 \cos\left(\frac{\alpha\pi}{2}\right)$$

$$ii. \eta = 0 \text{ and } \delta = -3/k$$

where  $\eta = (b_1 + k\delta - 1)(b_4 - k\delta - 1) - (b_3 - k\delta)(b_2 - k\delta)$  and  $\tau = b_1 + b_4 + 2(k\delta - 1)$ .

*Proof.* The Jacobian matrix of the system (1) is as follow

$$J[x_1, x_2, \varphi] = \begin{bmatrix} -1 + b_1 \text{sech}^2(x_1) + k\varphi & b_2 \text{sech}^2(x_2) - k\varphi & k(x_1 - x_2) \\ b_3 \text{sech}^2(x_1) - k\varphi & -1 + b_4 \text{sech}^2(x_2) + k\varphi & -k(x_1 - x_2) \\ 1 & -1 & 0 \end{bmatrix} \quad (9)$$

which at its equilibrium,  $E^* = [0, 0, \delta]$ , will be

$$J(E^*) = \begin{bmatrix} -1 + b_1 + k\delta & b_2 - k\delta & 0 \\ b_3 - k\delta & -1 + b_4 + k\delta & 0 \\ 1 & -1 & 0 \end{bmatrix}, \quad (10)$$

Thus, characteristic equation of matrix (10) will be in the form of  $p(\lambda) = \lambda p_1(\lambda)$  where

$$p_1(\lambda) = \lambda^2 + [-b_1 - b_4 + 2(1 - k\delta)]\lambda + (1 - b_1)(1 - b_4) - b_2b_3 + (b_1 + b_2 + b_3 + b_4 - 2)k\delta \quad (11)$$

Assuming  $\tau = -b_1 - b_4 + 2(1 - k\delta)$  and  $\eta = (1 - b_1)(1 - b_4) - b_2b_3 + (b_1 + b_2 + b_3 + b_4 - 2)k\delta$ , we can re-write the characteristic equation in the form of

$$p(\lambda) = \lambda(\lambda^2 - \tau\lambda + \eta)$$

According to lemma (2.2) then, the proof of (i) would be straightforward. Regarding case (ii), for  $\eta = 0$  and  $\delta = -3/k$ , the characteristic equation would have one zero root,  $\lambda_1 = 0$ , and one negative real root,  $\lambda_1 = -4.1$ . Based on lemma (2.1) therefore,  $E^*$  would be a stable point (Table 1).  $\square$

Table 1: Stability region of two-neuron FMHNN model (1) under  $b_1 = -0.1$ ,  $b_2 = 2.8$ ,  $b_3 = -3$ , and  $b_4 = 4$  assumption.

#	Conditions on parameters $(\eta, \tau, \delta)$			Stability conditions
Case 1	$\eta = 0$	—	$\delta = -3/k$	Stable
Case 2	$\eta > 0$	$\tau = 0$	$\delta = -0.95/k$	Stable
Case 3	$\eta > 0$	$\tau > 0$	$-0.95/k < \delta < 1.9512/k$	Stable
Case 4	$\eta > \tau^2/4$	$\tau < 0$	$-0.95/k < \delta < 1.9512/k$	$\cos(\frac{\alpha\pi}{2}) > \frac{\tau}{2\sqrt{\eta}}$
Case 5	$\eta < 0$	—	$\delta > 1.9512/k$ OR $\delta < -3/k$	Unstable

**Remark 2.2.** When  $\eta < 0$  then  $\tau^2 - 4\eta > 0$  and  $\delta > 1.9512/k$  or  $\delta < -3/k$ . Therefore,  $\lambda_{1,2}$  has at least one positive real root, which shows  $E^*$  is an unstable point.

#### Specified Scenario: Example I

Same as Chen et al [43], we set  $b_1 = -0.1$ ,  $b_2 = 2.8$ ,  $b_3 = -3$  and  $b_4 = 4$  in system (1). At the equilibrium point thus, the characteristic equation (11) reduces to

$$P(\lambda) = \lambda [\lambda^2 - (1.9 + 2k\delta)\lambda + 5.1 + 1.7k\delta],$$

Through assumption of  $\tau = -(1.9 + 2k\delta)$ ,  $\eta = 5.1 + 1.7k\delta$ , and  $k = 0.15$  in Theorem (2.4), Table (1) simplifies into Table (2). Note that the stability criteria of model (1) is calculated in upper and lower bound of  $\delta$  value.

#### 2.2.4. Stability of FMHNN Model with Ring Structure

**Theorem 2.5.** The system (3) is locally asymptotically stable at its equilibrium point,  $X^* = (0, 0, \phi^*)$ , when  $1 < n < (2p(d + 1) + d)/d$  and  $0 < \alpha < 1$  (Table 3).

*Proof.* First we re-write the system (3) in the compact form as below

$$\mathbb{F}(X) = AX + \mathbb{H}(X) \tag{12}$$

where  $\mathbb{H}(X) = B_1 \tanh(x_1) + B_2 \tanh(x_2) + \varphi KX$ ,  $A = bcirc(A_0, A_1, \dots, A_1) \in \mathbb{R}^{n \times n}$ ,  $B_1 = [\beta_1]_{1 \times n}$ ,  $B_2 = [\beta_2]_{1 \times n}$ ,  $\beta_1 = [b_1, b_3, 0]$ ,  $\beta_2 = [b_2, b_4, 0]$ , and  $K = bcirc(\kappa, 0, \dots, 0)_{1 \times n}$  so that

Table 2: The amount of eigenvalues for the stability region according table (1) when  $k = 0.15$  in FMHNN model (1).

#	$\delta$	Equilibrium	Eigenvalues $\lambda_{1,2}$	Could be stable in	
				integer case?	fractional case?
Case 1	-20	(0, 0, -20)	0.00, -4.10	No	No
Case 2	-6.3	(0, 0, -6.3)	$0.00 \pm 1.87i$	No	Yes
Case 3	-18	(0, 0, -18)	-3.35, -0.15	Yes	Yes
Case 3	-8.0	(0, 0, -8.0)	$-0.25 \pm 1.73i$	Yes	Yes
Case 4	-5.0	(0, 0, -5.0)	$0.20 \pm 1.95i$	No	Yes
Case 4	10	(0, 0, 10)	$2.45 \pm 1.28i$	No	Yes
Case 5	14	(0, 0, 14)	3.85, 2.25	No	No
Case 5	-25	(0, 0, -25)	0.21, -5.82	No	No

$A_0, A_1 \in \mathbb{R}^{3 \times 3}$  and

$$A_0 = \begin{bmatrix} -1 - \frac{d}{p} & 0 & 0 \\ 0 & -1 & 0 \\ 1 & -1 & 0 \end{bmatrix}, \quad A_1 = \begin{bmatrix} \frac{d}{2p} & 0 & 0 \\ 0 & 0 & 0 \\ 0 & 0 & 0 \end{bmatrix}, \quad \kappa = \begin{bmatrix} -k & k & 0 \\ k & -k & 0 \\ 0 & 0 & 0 \end{bmatrix}$$

Next we show that equation (12) satisfies stability condition at its equilibrium point,  $X^* = (0, 0, \phi^*)$  because

$$\lim_{X \rightarrow X^*} \frac{\|\mathbb{H}(X)\|}{\|X - X^*\|} = \lim_{X \rightarrow X^*} \frac{(\|B_1\| \|\tanh(x_1)\| + \|B_2\| \|\tanh(x_2)\| + \|\varphi\| \|K\| \|X\|)}{\|X - X^*\|} = 0$$

which this satisfies one of conditions of theorem (2.2.2). The other condition also holds when  $1 < n < (2p(d+1) + d)/d$  and  $0 < \alpha < 1$  because

$$\begin{aligned} \det(A - \lambda I) &= \{\lambda(A_0 + (n-1) \times A_1), \lambda(A_0 - A_1) \times (n-1)\} \\ &= \left\{ -1, 0, \frac{d(n-1) - 2p(d+1)}{2p}, 1-n, 0, (1-n)(3d/2p + 1) \right\} \end{aligned}$$

□

Table 3: Stability region of FMHNN model (3). No condition is applied to the memristor variable,  $\phi^*$ , at equilibrium.

Conditions on	
NO. of sub-networks	Fractional order
$1 < n < (2p(d+1) + d)/d$	$0 < \alpha < 1$

**Remark 2.3.** For  $\alpha = 1$ , under the assumption of  $1 < n < (2p(d+1) + d)/d$  at equilibrium point,  $X^* = (0, 0, \phi^*)$ , the system (3) would have limit cycles.

**Specified Scenario: Example II**

In addition to our parameter assumption in the FMHNN model, we set  $p = 1$ , and  $d = 0.5$ . According to the compact form of model (12) then, we would have  $\beta_1 = [-0.1, -3, 0]$ ,  $\beta_2 = [2.8, 4, 0]$  and

$$A_0 = \begin{bmatrix} -1.1 & 0 & 0 \\ 0 & -1 & 0 \\ 1 & -1 & 0 \end{bmatrix}, A_1 = \begin{bmatrix} 0.05 & 0 & 0 \\ 0 & 0 & 0 \\ 0 & 0 & 0 \end{bmatrix}, \kappa = \begin{bmatrix} -0.15 & 0.15 & 0 \\ 0.15 & -0.15 & 0 \\ 0 & 0 & 0 \end{bmatrix} \quad (13)$$

This parameter assumption satisfies the stability criteria represented by theorem (2.5) when

$$1 < n < (2(1)(1 + 0.5) + 0.5)/0.5 = 7 \quad (14)$$

**2.2.5. Numerical Analysis**

We used FDE12 package [49] to find the solution for the models. FDE12 is a package written in Matlab that numerically solves the fractional ordinary differential equations. All the figures and numerical simulations are done by MATLAB programming language.

### 3. Results

**FMHNN Model.** We specified our theoretical calculations (Table. 1) through the same parameterization as Chen et al [43], calculated the eigenvalues for the model (1), and compared the integer,  $\alpha = 1$ , and non-integer,  $0 < \alpha < 1$ , case with each other (Table. 2). In the integer case, the null solution is not asymptotically stable for all cases but case 3 because of non-negative eigenvalues, while this is not the case when  $0 < \alpha < 1$ . For case 2,  $\delta = -6.3$ , the system (1) is asymptotically stable when  $\alpha \in (0, 1)$  as lemma (2.1) holds for this range. With regard to case 4 that  $-6.3 < \delta < 13$ , we examined two equilibrium points ( $\delta = -5$  and  $\delta = 10$ ). According to the amount of eigenvalues ( $\lambda_{1,2}$ ), given in Table (2), at the equilibrium points  $E_1^* = (0, 0, -5)$  and  $E_2^* = (0, 0, 10)$ , the stability condition (2.1) satisfies when  $\alpha < 0.9348$  and  $\alpha < 0.307$  respectively. As for case 5, we similarly looked into two equilibrium points ( $\delta = 14$  and  $\delta = -25$ ). The system is not stable in any of these two cases because the stability criteria are violated due to having positive real roots for the characteristic equation. The asymptotical stability comparison of integer and non-integer cases is summarised in Table (2).

We next tested the calculations numerically. From the phase plane simulation for case 4,  $\delta = -5$ , we can see that the dynamical behavior of the model is unstable for the integer case,  $\alpha = 1$ , and even for the non-integer case when  $\alpha = 0.97$  (Fig. 2, top), as the fractional order is greater than  $2|\arg(\lambda_{1,2})|/\pi$ , violating the stability criteria (2.1). However, when  $\alpha = 0.93$  which is somewhat less than 0.9348, the calculated value for the stability condition, the model output reaches the equilibrium point  $E^* = (0, 0, -5)$  over time (Fig. 2, bottom). Regardless of the stability condition, the  $\alpha$  parameter also

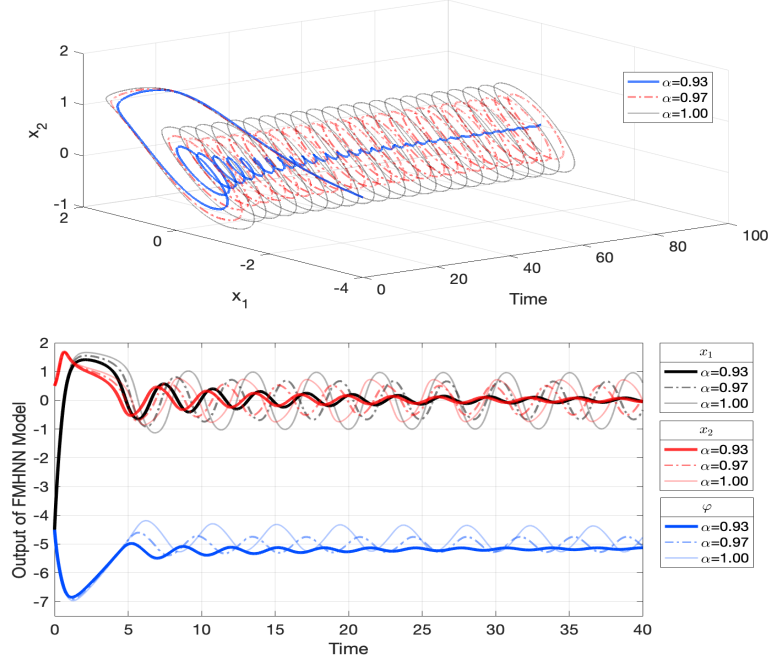


Figure 2: Phase diagrams and time series of FMHNN model (1) in Case 4,  $\delta = -5$ , with initial value  $(x_1(0), x_2(0), \varphi(0)) = (-4.5, 0.5, -4.5)$  for three different fractional orders. Details are given in the legends.

dampens out the overall dynamics of the model. Looking at the time series simulation (Fig. 2, bottom), we can see the shading dashed lines, representing  $\alpha = 0.97$ , have a smaller amplitude compared to the solid-shading lines, describing  $\alpha = 1.00$ .

As for the unstable region, case 5,  $\delta = 14$ , we observed that the model is unstable in both integer and non-integer cases (Fig. 3). It is, however, interesting that the fractional order could cause a delay in the dynamical transition of the model output. For  $\alpha = 0.75$ , the model starts with smooth destabilizing fluctuations after 20 seconds (Time > 20), while under the same condition for the model with  $\alpha = 0.85$  the oscillations start about 4 times sooner, Time  $\approx 5$ , (Fig. 3, bottom).

In our numerical analysis also, we noticed several striking coexisting multi-stable patterns and coexisting multiple attractors in the two-neuron-based FMHNN model (1). To elaborate upon that we performed three independent simulations using different initial values, showing the coexistence of several types of disconnected attractors due to periodic attractors with different periodicities, stable points, and unbounded divergent orbits which go to infinity. The phase plane and time series of coexisting multi-stable patterns of the attraction regions are shown in Fig. (4).

**FMHNN Model with Ring Structure.** In addition to considering the same model parameterization as Chen et al [43], we set  $(p, d) = (1, 0.5)$  and demonstrated that the stability of the model with ring structure (3) depends upon the number of sub-network,  $n$ . For  $n \geq 7$  we showed that the model is unstable, and we tested this through

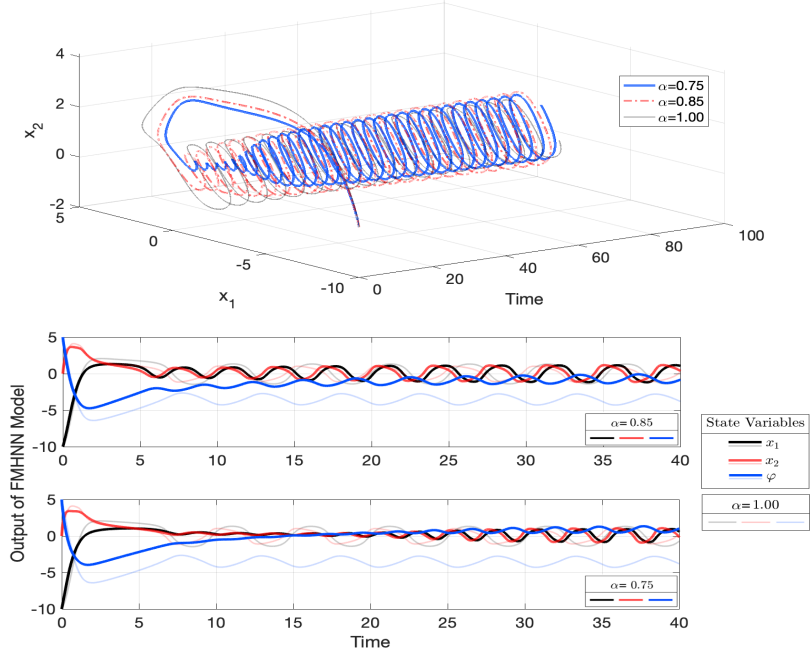


Figure 3: Phase diagrams and time series of FMHNN model (1) in case 5,  $\delta = 14$ , with initial value  $(x_1(0), x_2(0), \varphi(0)) = (-10, 10^{-6}, 5)$  for three different fractional orders. Details are given in the legends.

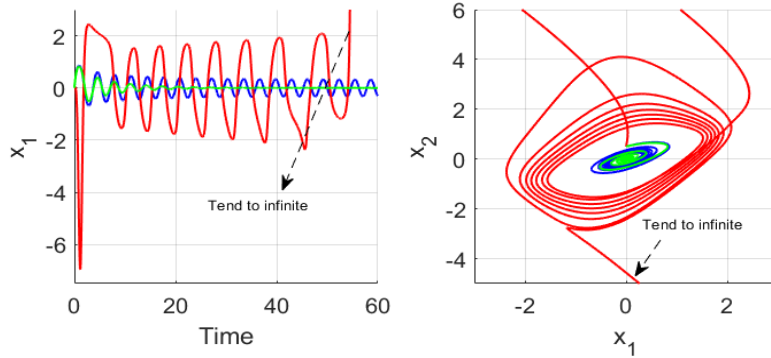


Figure 4: Coexisting multi-stable patterns of the attraction regions in the FMHNN model (1), with initial values  $X_{\text{blue}} = (0, 0.5, -5)$ ,  $X_{\text{red}} = (0, 0.5, 14)$ , and  $X_{\text{green}} = (0, 0.5, -6)$  for fractional order  $\alpha = 0.93$ .

solving the model numerically for  $n = 7$ , Fig. (5). From this figure, we notice that the  $\alpha$  parameter affects the amplitude of the oscillations. The smaller the alpha value, the smaller amplitude.

We also performed another simulation for  $n = 5$  where the model parameterization meets the asymptotic stability conditions (2.5). In this case, the model is stable when  $0 < \alpha < 1$ , (Fig. 6, top), and it would have stable limit cycles when  $\alpha = 1$  (Fig. 6,

bottom). We also examined the impact of  $\alpha$  parameter on the dynamical behavior of the model for  $n = 5$ . Although the model would be stable for all  $\alpha$  values in  $(0, 1)$  interval, under different  $\alpha$  values the trajectory of model output leads to various stationary points, Fig. (7). This indicates the importance of choosing the 'right'  $\alpha$  parameter in model implementation on real problems. Turing and parameter optimizations could give us an insight what the  $\alpha$  value must be [39].

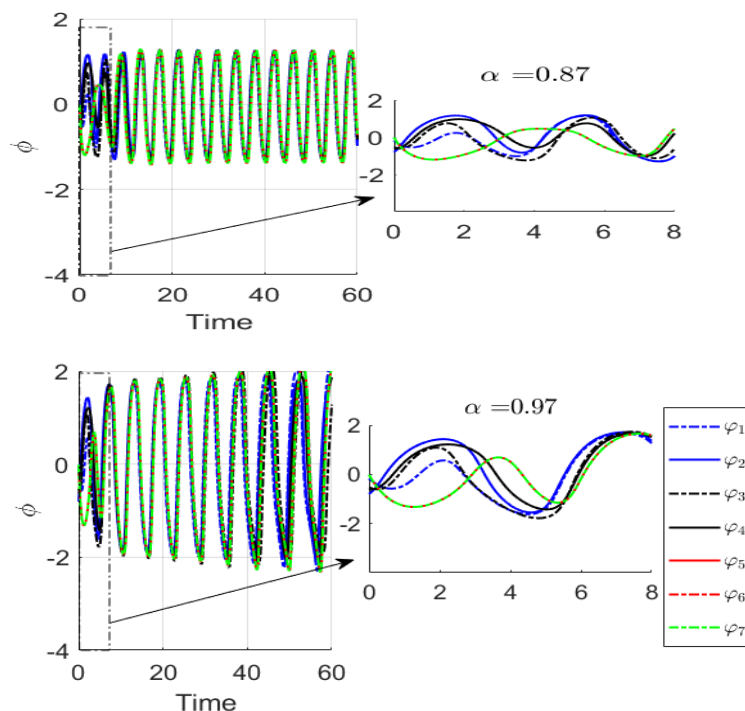


Figure 5: Time series of FMHNN model with ring structure (3) consisting of 7 sub-networks with  $p = 1$ ,  $d = 0.5$ ,  $N = 7$  and initial conditions  $X_1 = (-0.17, -0.80, -0.53, -0.63, -0.016, -0.11, -0.49)$ ,  $X_2 = (-0.39, -0.06, -0.41, -0.29, -0.98, -0.37, -0.34)$ ,  $\phi = (-0.83, -0.40, -0.66, -0.43, -0.17, -0.12, -0.95)$  for  $\alpha = 0.97$  and  $\alpha = 0.87$ .

**Bifurcation Analysis.** Here we would study the stability criteria further through investigating the influences of the initial conditions and the fractional-order parameter  $\alpha$  on our FMHNN model (1).

Again, we set  $b_1 = -0.1$ ,  $b_2 = 2.8$ ,  $b_3 = -3$  and  $b_4 = 4$  in system (1), as assumed by Chen et al [43]. Taking  $\alpha$  as the bifurcation parameter when  $\alpha \in [0.96, 1]$  and the initial value  $[0, 10^{-6}, 0]$ , we performed the bifurcation analysis. Figure (8) shows the bifurcation diagram of the  $\alpha - \phi$  plane, indicating that with the increase of  $\alpha$  value the trajectory of FMHNN evolves into unbounded behavior, chaos, eight-period cycles, four-period and finally to two-period cycles. Also according to the Lyapunov exponent shown in figure (8), the system can not be asymptotically stable for the given interval value of  $\alpha$ .

Next, we examined the impact of initial conditions on the dynamical transition of the model output by performing three independent simulations under different initial



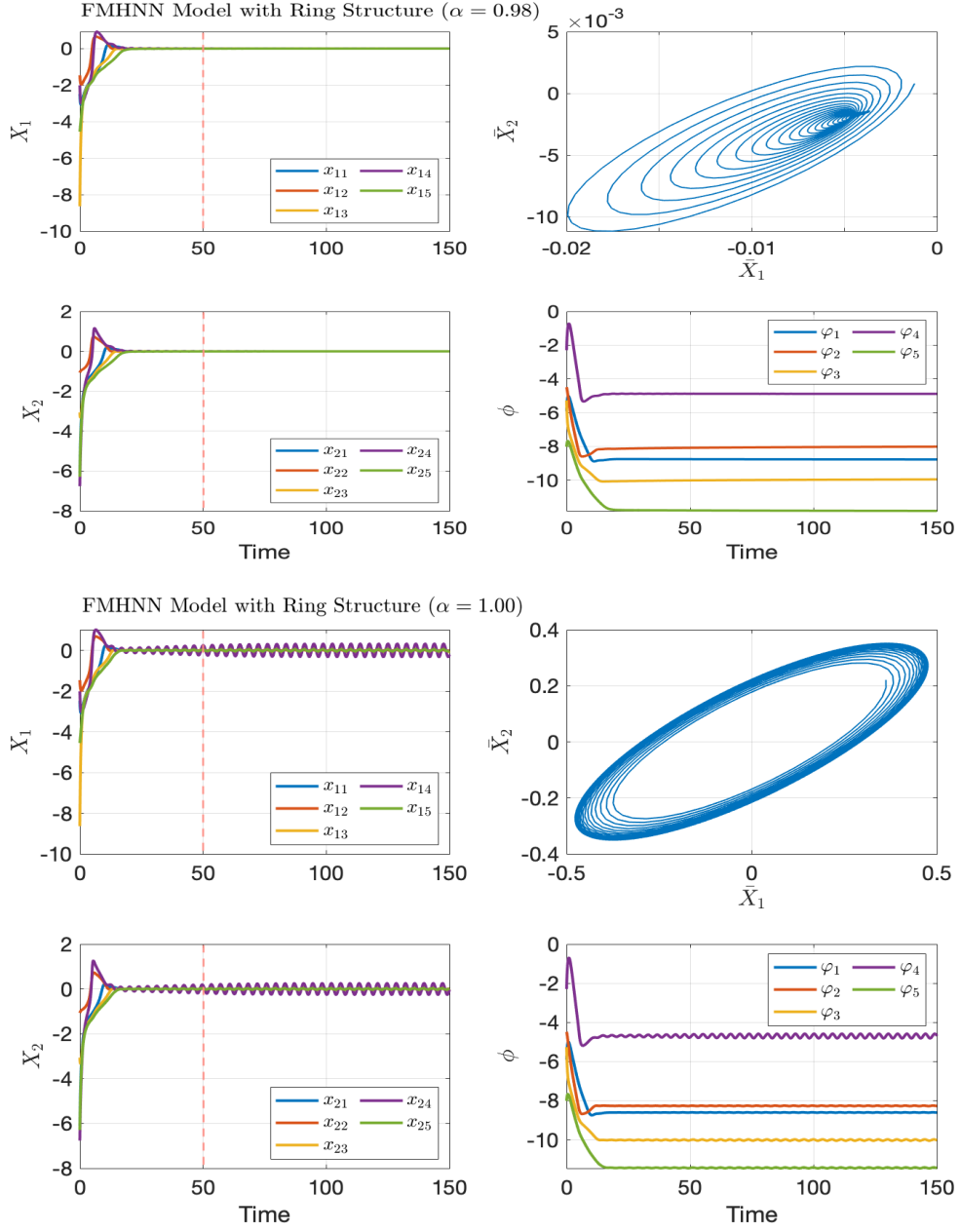


Figure 6: Phase diagrams and time series of FMHNN model with ring structure (3) consisting of 5 sub-networks with  $p = 1$ ,  $d = 0.5$  and initial condition  $X_1 = (-2.48, -6.12, -5.90, -1.46, -1.07)$ ,  $X_2 = (-4.48, -8.64, -3.06, -5.27, -2.01)$ ,  $\phi = (-6.76, -2.30, -4.55, -6.30, -8.02)$  where  $X_1 = [x_{1i}]$ ,  $X_2 = [x_{2i}]$ ,  $\phi = [\phi_i]$  for  $i = 1, \dots, 5$ .  $\bar{X}_1 = \frac{1}{5} \sum_{i=1}^5 x_{1i}$ , and  $\bar{X}_2 = \frac{1}{5} \sum_{i=1}^5 x_{2i}$  are average potentials between two neurons, calculated for  $t \geq 50$ . Further details are given in the titles and legends.

conditions:  $X_{\text{blue}} = [0.5, -1, 1]$ , the blue trajectory,  $X_{\text{red}} = [0.5, -0.5, 0.5]$ , the red

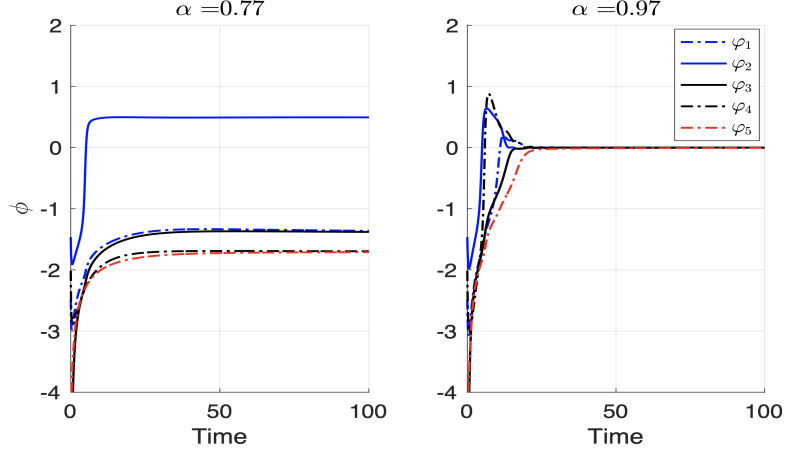


Figure 7: Time series of FMHNN model with ring structure (3) consisting of 5 sub-networks with  $p = 1$ ,  $d = 0.5$ ,  $N = 5$  and initial conditions  $X_1 = (-2.48, -6.12, -5.90, -1.46, -1.07)$ ,  $X_2 = (-4.48, -8.64, -3.06, -5.27, -2.01)$ ,  $\phi = (-6.76, -2.30, -4.55, -6.30, -8.02)$  for  $\alpha = 0.97$  and  $\alpha = 0.87$

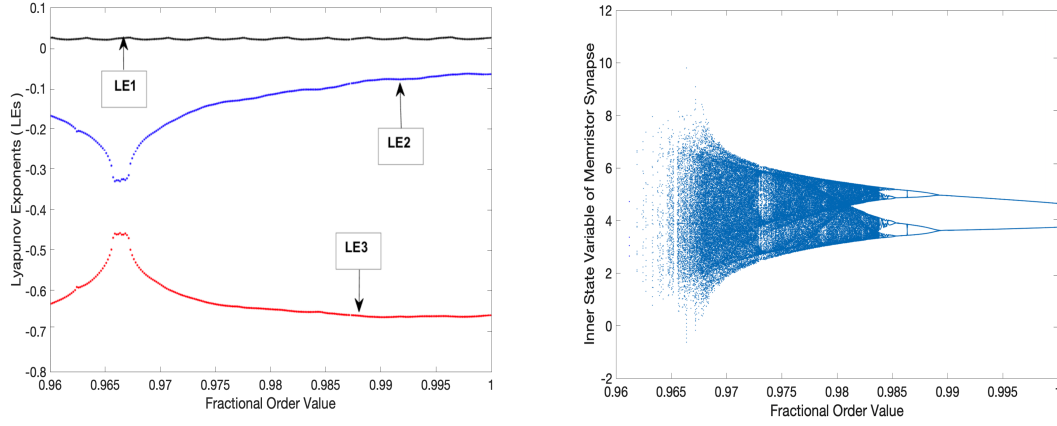


Figure 8: The bifurcation diagram and Lyapunov exponents of FMHNN model (1) on the  $\alpha - \phi$  plane over  $0.96 \leq \alpha \leq 1$  interval.

trajectory, and  $X_{\text{black}} = [0.5, -0.7, 0.7]$ , the black trajectory. From Fig. (9), we observed that under the  $X_{\text{red}}$  initial value, the trajectory of the FMHNN model (1) evolves from chaotic state into four-period cycles, then two-period and eventually into one-period cycles, while under the  $X_{\text{black}}$  initial value, we have different trajectories. The bifurcation patterns evolves from chaotic state into four-period cycles, two and then one-period, again two-period, and finally one-period cycles. Similar patterns is seen for the  $X_{\text{blue}}$  initial value (Fig. 9). This indicates the initial conditions could have an essential influence on the bifurcation behavior of the model.

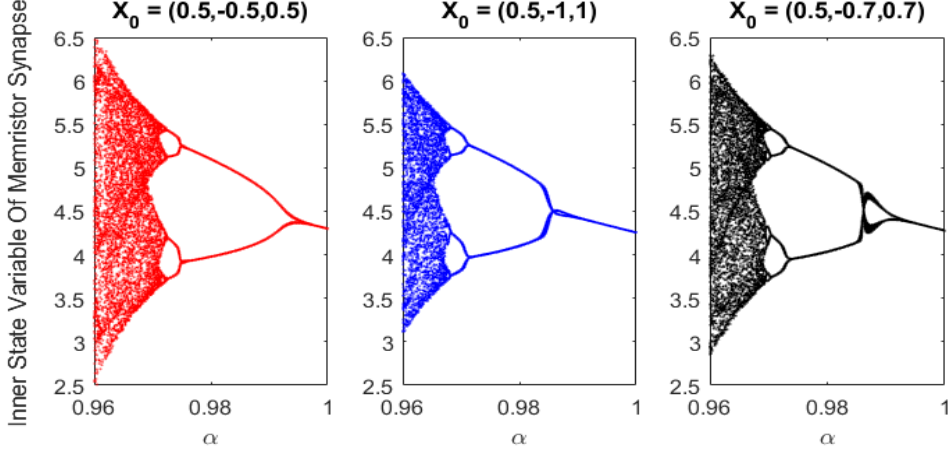


Figure 9: The bifurcation diagram of FMHNN model (1), under three different initial conditions  $X_{\text{red}} = (0.5, -0.5, 0.5)$ ,  $X_{\text{blue}} = (0.5, -1, 1)$  and  $X_{\text{black}} = (0.5, -0.7, 0.7)$ .

#### 4. Discussion and conclusion

A memristor is an electrical component restricting or regulating the flow of electrical current in a circuit. This component adds the magnetic flux to the membrane potential of a neuron model, enabling the system to remember the previous amount of charge that has flowed through it. Our FMHNN model extends this memory characteristic to keep the effect of all previous steps in the system. Due to the incorporated memory feature, the model shows more residence to changes compared to the MHNN model. The memory concept, coming from fractional derivative indeed, dampens out fluctuations in the model dynamic. Increasing the memory feature,  $\alpha \rightarrow 0$ , would lead the system as a whole settles on an equilibrium quicker (Fig. 10).

Our theoretical calculation indicates that the FMHNN model has a broader range in stability than the MHNN model. (Theory 2.4). Under the same parameterization as Chen et al [43], we verified this. Both models have five stability regions, among which the MHNN model is stable in only one area, while the FMHNN model could be stable in three areas (Table 1). Our numerical simulations also agree with this finding (Fig. 2), suggesting the memory concept could significantly influence the system dynamics.

It is noteworthy to notice that the FMHNN could not be stable for all ranges of  $\alpha \in (0, 1)$ . To highlight this, we performed bifurcation analyses and estimated Lyapunov exponents. The outputs show that the model experiences several dynamical transitions from unbounded to non-chaotic behaviour by increasing  $\alpha$  value from 0.96 to 1 (Fig. 8). When  $\alpha = 1$ , the model is also unstable as the stability condition is violated. Moreover, our simulations shows that the dynamical transitions of model can be affected by changing initial points (Fig. 9).

Next, we expanded the previous model to a general fractional-order network using the ring topology, where each membrane is in ring structure with  $n$  sub-networks, improving the synchronization within the synapse and increasing the network dimension.

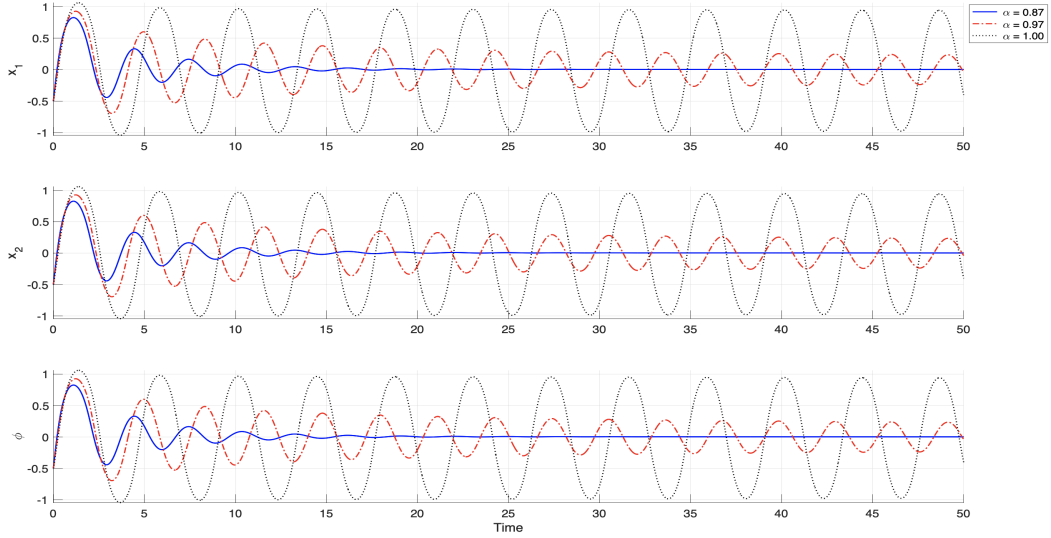


Figure 10: Time series of FMHNN model with initial condition  $X_0 = (-0.5, 0.25, -5)$ . The parameters are chosen from Chen et al [43].

We obtained the stability criteria, highlighting the importance of the synchronization factor in the network. In effect, we found that the stability does not only depend upon the memory element,  $\alpha$ , but it depends upon the number of sub-networks,  $n$ , in membranes (Table 3). For  $\alpha = 1$  also, the model would have stable limit cycles (Remark 2.3).

Within the same parameterization as the two-neuron network model, we tested our calculations for the fractional-order network including  $n$  units of the two-neuron network model which are connected in ring topology. The units are coupled by the nearest neighbourhood neurons with the coupling strength of  $d = 0.5$ . We found that the model cannot be stable when the network size exceeds  $n = 6$ . To check this numerically, we performed several simulations summarized below.

- $n = 5$  &  $0 < \alpha < 1$ , the system is stable (Fig. 6),
- $n = 5$  &  $\alpha = 1$ , the system has a stable limit cycle (Fig. 6),
- $n = 7$ , the system is unstable (Fig. 7).

Our simulations also suggest that the fractional-order value could affect the model dynamics significantly. In addition to dampening out the fluctuations in the model dynamics (Fig. 5), the  $\alpha$  value could shift the system as a whole settles on different equilibrium points (Fig. 7).

The number of sub-neurons, the units, plays a pivotal role in the stability condition. Neuronal networks could give us a better insight into the existing collective behaviours

of neurons by embedding the synapses in models where nodes are coupled in different types of synchronization. Due to the memory characteristic and enriching synchronized features of the fractional-order rig structure network, we think FMHNN models could be employed to design high-density artificial neural networks to examine complex systems like the brain. Although this work makes a solid mathematical framework to control the FMHNN model via stability analyses, there is more room for improvement. Therefore, it would be interesting to evaluate the impact of lag synchronization in the FMHNN model or to consider other types of synchronization, such as partial synchronization, phase synchronization, lag synchronization, cluster synchronization, and so forth in the model.

### Data availability statement

No data were used to support this study.

### Statements and Declarations

The authors did not receive support from any organization for the submitted work. Also they declare that they have no known competing financial interests or personal relationships that could have appeared to influence the work reported in this paper.

### Acknowledgment

MA expresses his appreciation for many enlightening conversations with *Prof. Andrew J. Irwin* of Dalhousie University during the revision process.

### References

- [1] Q. Li and X. Yang, “Complex dynamics in a simple Hopfield-type neural network,” in *International Symposium on Neural Networks*, pp. 357–362, Springer, 2005.
- [2] G. Gaurav, R. S. Anand, and V. Kumar, “Eeg based cognitive task classification using multifractal detrended fluctuation analysis,” *Cognitive Neurodynamics*, vol. 15, no. 6, pp. 999–1013, 2021.
- [3] S. Nobukawa, T. Yamanishi, H. Nishimura, Y. Wada, M. Kikuchi, and T. Takahashi, “Atypical temporal-scale-specific fractal changes in Alzheimer’s disease eeg and their relevance to cognitive decline,” *Cognitive neurodynamics*, vol. 13, no. 1, pp. 1–11, 2019.
- [4] S. Nobukawa, N. Wagatsuma, and H. Nishimura, “Deterministic characteristics of spontaneous activity detected by multi-fractal analysis in a spiking neural network with long-tailed distributions of synaptic weights,” *Cognitive Neurodynamics*, vol. 14, no. 6, pp. 829–836, 2020.

- [5] M. A. Matlob and Y. Jamali, “The concepts and applications of fractional order differential calculus in modeling of viscoelastic systems: a primer,” *Critical Reviews™ in Biomedical Engineering*, vol. 47, no. 4, 2019.
- [6] C. Zúñiga-Aguilar, H. Romero-Ugalde, J. Gómez-Aguilar, R. Escobar-Jiménez, and M. Valtierra-Rodríguez, “Solving fractional differential equations of variable-order involving operators with Mittag-Leffler kernel using artificial neural networks,” *Chaos, Solitons & Fractals*, vol. 103, pp. 382–403, 2017.
- [7] C. Zúñiga-Aguilar, A. Coronel-Escamilla, J. Gómez-Aguilar, V. Alvarado-Martínez, and H. Romero-Ugalde, “New numerical approximation for solving fractional delay differential equations of variable order using artificial neural networks,” *The European Physical Journal Plus*, vol. 133, no. 2, pp. 1–16, 2018.
- [8] P.-Y. Xiong, H. Jahanshahi, R. Alcaraz, Y.-M. Chu, J. Gómez-Aguilar, and F. E. Alsaadi, “Spectral entropy analysis and synchronization of a multi-stable fractional-order chaotic system using a novel neural network-based chattering-free sliding mode technique,” *Chaos, Solitons & Fractals*, vol. 144, p. 110576, 2021.
- [9] C. Zúñiga-Aguilar, J. Gómez-Aguilar, H. Romero-Ugalde, H. Jahanshahi, and F. E. Alsaadi, “Fractal-fractional neuro-adaptive method for system identification,” *Engineering with Computers*, pp. 1–24, 2021.
- [10] C. Zúñiga-Aguilar, J. Gómez-Aguilar, H. Romero-Ugalde, R. Escobar-Jiménez, G. Fernández-Anaya, and F. E. Alsaadi, “Numerical solution of fractal-fractional Mittag-Leffler differential equations with variable-order using artificial neural networks,” *Engineering with Computers*, pp. 1–14, 2021.
- [11] C. Z. Aguilar, J. Gómez-Aguilar, V. Alvarado-Martínez, and H. Romero-Ugalde, “Fractional order neural networks for system identification,” *Chaos, Solitons & Fractals*, vol. 130, p. 109444, 2020.
- [12] S. He, “Complexity and chimera states in a ring-coupled fractional-order memristor neural network,” *Front. Appl. Math. Stat.* 6: 24. doi: 10.3389/fams, 2020.
- [13] Z. Njitacke, J. Kengne, and H. Fotsin, “A plethora of behaviors in a memristor based Hopfield neural networks (hnns),” *International Journal of Dynamics and Control*, vol. 7, no. 1, pp. 36–52, 2019.
- [14] Q. Li, X.-S. Yang, and F. Yang, “Hyperchaos in Hopfield-type neural networks,” *Neurocomputing*, vol. 67, pp. 275–280, 2005.
- [15] P. C. Rech, “Period-adding and spiral organization of the periodicity in a Hopfield neural network,” *International Journal of Machine Learning and Cybernetics*, vol. 6, no. 1, pp. 1–6, 2015.
- [16] H. Korn and P. Faure, “Is there chaos in the brain? II. Experimental evidence and related models,” *Comptes rendus biologies*, vol. 326, no. 9, pp. 787–840, 2003.

- [17] A. Srinivasulu, “Digital very-large-scale integration (VLSI) hopfield neural network implementation on field programmable gate arrays (FPGA) for solving constraint satisfaction problems,” *Journal of Engineering and Technology Research*, vol. 4, no. 1, pp. 11–21, 2012.
- [18] G. Joya, M. Atencia, and F. Sandoval, “Hopfield neural networks for optimization: study of the different dynamics,” *Neurocomputing*, vol. 43, no. 1-4, pp. 219–237, 2002.
- [19] A. Thomas, “Memristor-based neural networks,” *Journal of Physics D: Applied Physics*, vol. 46, no. 9, p. 093001, 2013.
- [20] X. Hu and C. Liu, “Dynamic property analysis and circuit implementation of simplified memristive Hodgkin–Huxley neuron model,” *Nonlinear Dynamics*, vol. 97, no. 2, pp. 1721–1733, 2019.
- [21] A. Mazarei, M. A. Matlob, G. Riazi, and Y. Jamali, “The role of topology in the synchronization of neuronal networks based on the Hodgkin-Huxley model,” *arXiv preprint arXiv:1812.02297*, 2018.
- [22] K. Usha and P. Subha, “Hindmarsh-rose neuron model with memristors,” *Biosystems*, vol. 178, pp. 1–9, 2019.
- [23] C. Morris and H. Lecar, “Voltage oscillations in the barnacle giant muscle fiber,” *Biophysical journal*, vol. 35, no. 1, pp. 193–213, 1981.
- [24] K. Li, H. Bao, H. Li, J. Ma, Z. Hua, and B. Bao, “Memristive Rulkov neuron model with magnetic induction effects,” *IEEE Transactions on Industrial Informatics*, vol. 18, no. 3, pp. 1726–1736, 2021.
- [25] Q. Xu, Z. Ju, S. Ding, C. Feng, M. Chen, and B. Bao, “Electromagnetic induction effects on electrical activity within a memristive Wilson neuron model,” *Cognitive Neurodynamics*, pp. 1–11, 2022.
- [26] Y. Yang, J. Ma, Y. Xu, and Y. Jia, “Energy dependence on discharge mode of Izhikevich neuron driven by external stimulus under electromagnetic induction,” *Cognitive Neurodynamics*, vol. 15, no. 2, pp. 265–277, 2021.
- [27] H. Bao, A. Hu, W. Liu, and B. Bao, “Hidden bursting firings and bifurcation mechanisms in memristive neuron model with threshold electromagnetic induction,” *IEEE Transactions on Neural Networks and Learning Systems*, vol. 31, no. 2, pp. 502–511, 2019.
- [28] Q. Xu, S. Ding, H. Bao, M. Chen, and B. Bao, “Piecewise-linear simplification for adaptive synaptic neuron model,” *IEEE Transactions on Circuits and Systems II: Express Briefs*, 2021.

- [29] J. Chen, Z. Zeng, and P. Jiang, “Global Mittag-Leffler stability and synchronization of memristor-based fractional-order neural networks,” *Neural Networks*, vol. 51, pp. 1–8, 2014.
- [30] X. F. Wang and G. Chen, “Complex networks: small-world, scale-free and beyond,” *IEEE circuits and systems magazine*, vol. 3, no. 1, pp. 6–20, 2003.
- [31] S. Kazemi and Y. Jamali, “Phase synchronization and measure of criticality in a network of neural mass models,” *Scientific Reports*, vol. 12, no. 1, pp. 1–18, 2022.
- [32] Y.-S. Chen, T.-H. Lin, and S.-M. Lin, “Raa: a ring-based address autoconfiguration protocol in mobile ad hoc networks,” *Wireless personal communications*, vol. 43, no. 2, pp. 549–571, 2007.
- [33] R. Mêwanou and S. Pierre, “Link-state-based algorithms for dynamic routing in all-optical networks with ring topologies,” *Photonic Network Communications*, vol. 11, no. 1, pp. 5–14, 2006.
- [34] Y. Tang, Z. Wang, and J.-a. Fang, “Pinning control of fractional-order weighted complex networks,” *Chaos: An Interdisciplinary Journal of Nonlinear Science*, vol. 19, no. 1, p. 013112, 2009.
- [35] C. Jiang, F. Zhang, and T. Li, “Synchronization and antisynchronization of N-coupled fractional-order complex chaotic systems with ring connection,” *Mathematical Methods in the Applied Sciences*, vol. 41, no. 7, pp. 2625–2638, 2018.
- [36] M. M. Amirian, I. Towers, Z. Jovanoski, and A. J. Irwin, “Memory and mutualism in species sustainability: A time-fractional lotka-volterra model with harvesting,” *Heliyon*, vol. 6, no. 9, p. e04816, 2020.
- [37] M. Khalighi, L. Eftekhari, S. Hosseinpour, and L. Lahti, “Three-species Lotka-Volterra model with respect to Caputo and Caputo-Fabrizio fractional operators,” *Symmetry*, vol. 13, no. 3, p. 368, 2021.
- [38] M. Saeedian, M. Khalighi, N. Azimi-Tafreshi, G. Jafari, and M. Ausloos, “Memory effects on epidemic evolution: The susceptible-infected-recovered epidemic model,” *Physical Review E*, vol. 95, no. 2, p. 022409, 2017.
- [39] M. Khalighi, D. Gonze, K. Faust, G. Sommeria-Klein, and L. Lahti, “Quantifying the impact of ecological memory on the dynamics of interacting communities,” *bioRxiv*, 2021.
- [40] M. M. Amirian, A. J. Irwin, and Z. V. Finkel, “Extending the Monod model of microbial growth with memory,” *arXiv preprint arXiv:2207.02028*, 2022.
- [41] M. Khalighi, M. Amirianmatlob, and A. Malek, “A new approach to solving multiorder time-fractional advection–diffusion–reaction equations using BEM and Chebyshev matrix,” *Mathematical Methods in the Applied Sciences*, vol. 44, no. 4, pp. 2964–2984, 2021.



- [42] I. Podlubny, *Fractional differential equations: an introduction to fractional derivatives, fractional differential equations, to methods of their solution and some of their applications*. Elsevier, 1998.
- [43] C. Chen, J. Chen, H. Bao, M. Chen, and B. Bao, “Coexisting multi-stable patterns in memristor synapse-coupled Hopfield neural network with two neurons,” *Nonlinear Dynamics*, vol. 95, no. 4, pp. 3385–3399, 2019.
- [44] A. Kaveh and H. Rahami, “Block circulant matrices and applications in free vibration analysis of cyclically repetitive structures,” *Acta Mechanica*, vol. 217, no. 1, pp. 51–62, 2011.
- [45] G. J. Tee, “Eigenvectors of block circulant and alternating circulant matrices,” *New Zealand Journal of Mathematics*, vol. 36, no. 8, pp. 195–211, 2007.
- [46] D. Matignon, “Stability results for fractional differential equations with applications to control processing,” in *Computational engineering in systems applications*, vol. 2, pp. 963–968, Lille, France, 1996.
- [47] E. Kaslik and S. Sivasundaram, “Nonlinear dynamics and chaos in fractional-order neural networks,” *Neural Networks*, vol. 32, pp. 245–256, 2012.
- [48] X.-J. Wen, Z.-M. Wu, and J.-G. Lu, “Stability analysis of a class of nonlinear fractional-order systems,” *IEEE Transactions on circuits and systems II: Express Briefs*, vol. 55, no. 11, pp. 1178–1182, 2008.
- [49] R. Garrappa, “Numerical solution of fractional differential equations: A survey and a software tutorial,” *Mathematics*, vol. 6, no. 2, p. 16, 2018.